Journal of Alloys and Compounds 508 (2010) 359–363

Contents lists available at ScienceDirect

Journal of Alloys and Compounds

journal homepage: www.elsevier.com/locate/jallcom

High temperature deformability and microstructural evolution of Ti–47Al–2Cr–0.2Mo alloy

Huizhong Li[a,*], Zhou Li[a], Wei Zhang[b], Yan Wang[b], Yong Liu[b], Haijun Wang[a]

[a] School of Materials Science and Engineering, Central South University, Changsha 410083, China
[b] State Key Laboratory of Powder Metallurgy, Central South University, Changsha 410083, China

ARTICLE INFO

Article history:
Received 14 April 2010
Received in revised form 3 June 2010
Accepted 10 June 2010
Available online 30 June 2010

Keywords:
Ti–47Al–2Cr–0.2Mo alloy
Engineering strain
Flow stress
DRX
EBSD

ABSTRACT

High temperature deformability and microstructural evolution of Ti–47Al–2Cr–0.2Mo alloy were studied by using a Gleeble-1500 simulated machine at temperature from 1050 °C to 1150 °C with strain rate from 2.5 s^{-1} to 7.5 s^{-1} and engineering compressive strain from 20% to 50%. The results indicate that the largest engineering compressive strain of the alloy increases with decreasing strain rate and increasing deformation temperature. It has been shown that the strain rate affects the largest engineering compressive strain of the alloy effectively. High temperature deformation mechanism of Ti–47Al–2Cr–0.2Mo alloy mainly refers to the bending and fracturing of the lamellar structures and dynamic recrystallization (DRX). Electron back scattered diffraction (EBSD) and transmission electron microscopic (TEM) results reveal the DRX mostly occurring at grains boundary and interlamellar spacing at a strain rate of 7.5 s^{-1} is much finer than that at a strain rate of 2.5 s^{-1} at 1150 °C.

1. Introduction

TiAl-based alloys are widely used as high temperature structural materials in many fields (e.g., aerospace and automotive industries) because of their attractive properties, such as low density, high specific strength, high specific stiffness, good oxidation resistance, high resistance to oxidation and good creep properties at high temperature [1–7]. However, the low room temperature ductility and poor formability limit the extensive application of TiAl-based alloys [8]. During last decades, considerable efforts have been devoted to improve the both room temperature ductility and formability [6]. One of the best ways to improve the alloys' ductility is to convert the coarse grained, texture and segregated microstructure into a more homogeneous and fine-grained microstructure by hot forging [9].

In recent years, many researches have been carried out to improve the alloys' ductility through microstructure control using the hot deformation process [10–12] and refining near-gamma grains and/or the lamellar colonies [13,14]. Hot deformation behaviors of TiAl-based alloys are mainly affected by the deformation temperature, strain rate, engineering compressive strain, and stress condition. The material deformability can be improved by changing the processing parameters [15]. He et al. [8] investigated the effects of deformation temperature and strain rate on the hot deformation characteristics of as-cast Ti–45Al–8.5Nb–(W,B,Y) alloy at the temperature of 1100–1200 °C with strain rates from 10^{-3} s^{-1} to 10^{-1} s^{-1}. They indicated that the flow stress of the alloy increases with the increase of strain rate and decrease of deformation temperature. Xu et al. [16] studied deformability and microstructure transformation of pilot ingots of Ti–45Al–(8–9)Nb–(W,B,Y) alloy at the temperature from 900 °C to 1250 °C and at a nominal strain rate range from 5×10^{-4} s^{-1} to 1 s^{-1}. They established the deformation map and investigated the influence of the deformation on the microstructure of the alloy. So far, there is no study of the deformability of Ti–Al–Cr–Mo alloy at higher strain rates (from 2.5 s^{-1} to 7.5 s^{-1}). Generally, the higher strain rate is not suitable for the hot deformability, but the higher strain rate can reduce the forging time which can decrease temperature drop and the higher strain rate is good for obtaining fine-grains.

In this study, the effects of deformation temperature and the strain rate at high level on hot deformability and microstructural evolution of Ti–47Al–2Cr–0.2Mo alloy were investigated by isothermal hot compression and the highest engineering compressive strain of the alloy were recorded in different deformation conditions.

2. Experimental

The alloy powders with a nominal composition of Ti–47Al–2Cr–0.2Mo (at.%) were produced by plasma rotating electrode process (PREP). Alloy powder of particle size 100–150 μm was filled into steel can and degassed at 400 °C, then processed by hot isostatic pressing (HIP) at 1200 °C for 4 h with a pressure of 170 MPa. Cylindrical compacts with the dimensions of approximately Φ50 mm × 100 mm and high relative density of more than 99.6% were obtained. Pieces with a diameter of 10 mm and a height of 12 mm were cut by electric-discharge machining. The prepared

* Corresponding author. Tel.: +86 731 88830377; fax: +86 731 88830257.
E-mail address: lhz606@mail.csu.edu.cn (H. Li).

0925-8388/$ – see front matter © 2010 Elsevier B.V. All rights reserved.
doi:10.1016/j.jallcom.2010.06.124

specimens were deformed by upsetting using a Gleeble 1500 thermal simulation machine at temperature from 1050 °C to 1150 °C with a strain rate from 2.5 s^{-1} to 7.5 s^{-1} and engineering compressive strains from 20% to 50%. The samples were heated by a resistance furnace to the deformed temperature with a heating rate of 5 °C s^{-1} using thermocoupled feedback-controlled AC current. Before deformation process, the samples were homogenized for 180 s at the deformed temperature. The variations of true stress and true strain were obtained from the controlling computer equipped with an automatic data acquisition system. In order to reduce the frictional force between the press indenters and the specimens, a graphite lubricant was used during the isothermal compression tests. The qualities of the samples compressed to different engineering strains at various strain rates and temperatures were evaluated. The largest engineering compressive strains, which were defined as the engineering strain corresponding to the compressed samples without fracture, were thus obtained.

The microstructure of the deformed specimens was examined using Sirion200 scanning electron microscope (SEM) and Tecnai G^2 20 TEM. The EBSD technique was used to measure the local crystal orientations of the processed specimens. The resulting specimen was electropolished and examined using a SEM with XM4-Hikari. Measurements were conducted at intervals of 0.3 μm for the mid-plane section of the specimens. The accumulated EBSD data were treated with TSL OIM 5.31 software to generate orientation map.

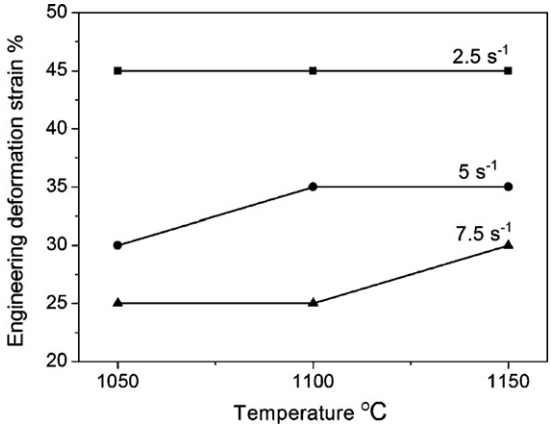

Fig. 1. The largest engineering compressive strain of the alloy.

3. Results and discussion

3.1. High temperature deformation

Fig. 1 shows the largest engineering compressive strain of the tested alloy with various strain rates at different deformation temperatures. When the engineering compressive strain is higher than the largest engineering compressive strain the samples will crack. It has been shown that the largest engineering compressive strain of the alloy increases with decreasing strain rate and increasing deformation temperature. At strain rate of 2.5 s^{-1}, the high quality forged samples can be obtained even strained up to 45%. No external and internal cracks are found for all the samples. As increasing strain rate, the largest engineering compressive strain of the alloy decreases obviously. When the strain rate is up to 7.5 s^{-1}, the largest engineering compressive strain decreases to 25% at 1050 °C. The results indicate that the strain rate affects the largest engineering compressive strain of the alloy effectively.

3.2. Flow stress

The true stress–strain curves at different deformation conditions which indicate the effects of deformation temperature and strain rate on flow behavior of the experimental alloy are shown in Fig. 2. It has been shown that the temperature and strain rate have a significant influence on the flow processes. The flow stresses firstly increase with increasing strain and reach a peak quickly, then as work softening overtakes work hardening, the flow stress decreases. The stress becomes steady when equilibrium of work softening and work hardening is obtained at strain rate of 2.5 s^{-1}.

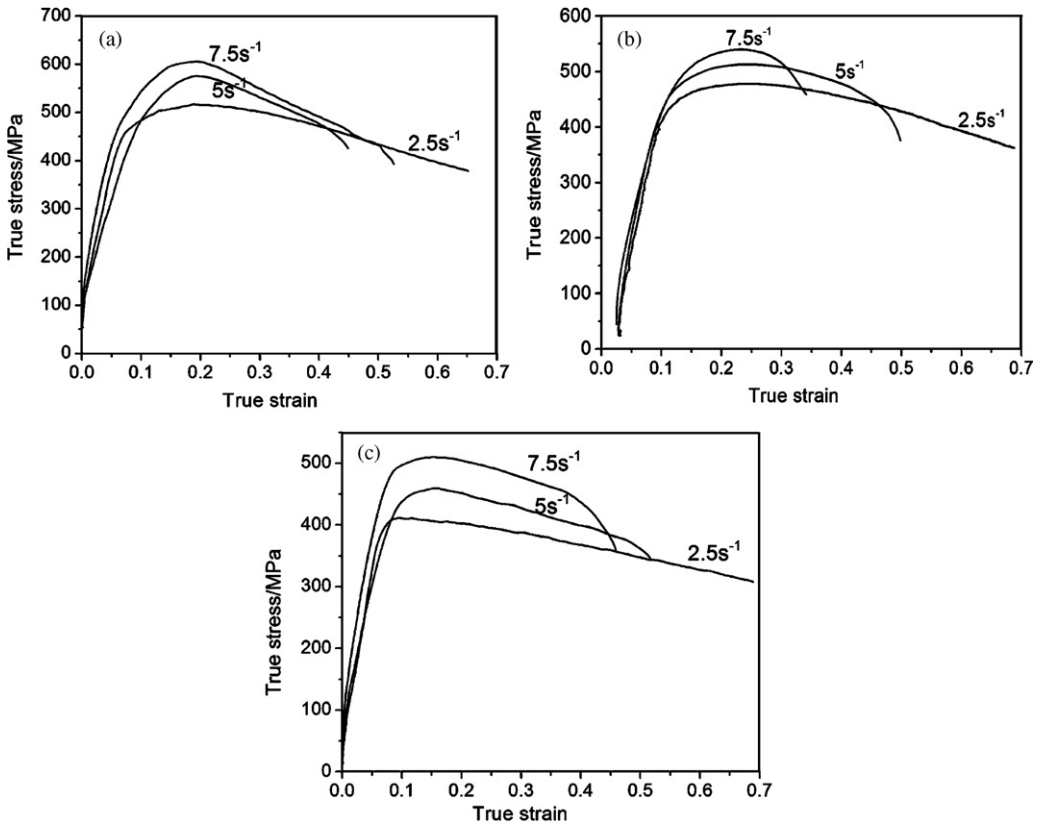

Fig. 2. Curves of true stress–true strain at temperature of (a) 1050 °C, (b) 1100 °C, and (c) 1150 °C.

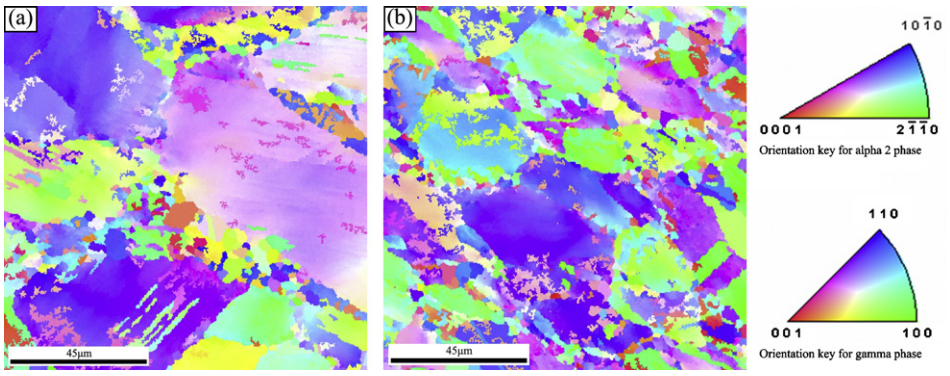

Fig. 3. EBSD orientation maps obtained from the specimens deformed at a 1150 °C and (a) at a strain rate of 2.5 s^{-1} and engineering strain of 45%, (b) at a strain rate of 7.5 s^{-1} and engineering strain of 30%.

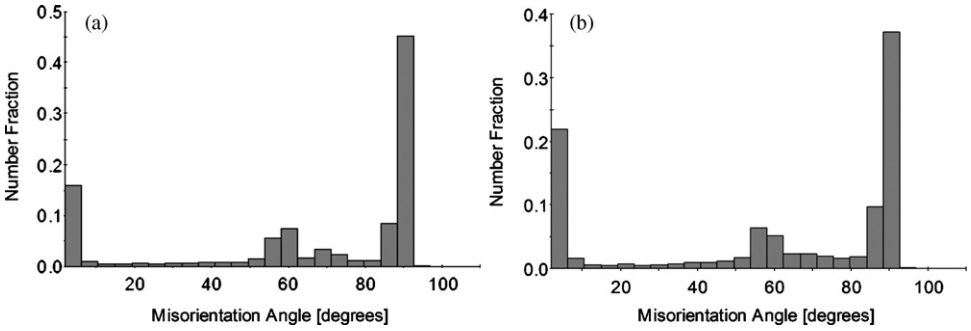

Fig. 4. Misorientation angle distribution obtained from the specimens deformed at 1150 °C and (a) at a strain rate of 2.5 s^{-1} and engineering strain of 45%, (b) at a strain rate of 7.5 s^{-1} and engineering strain of 30%.

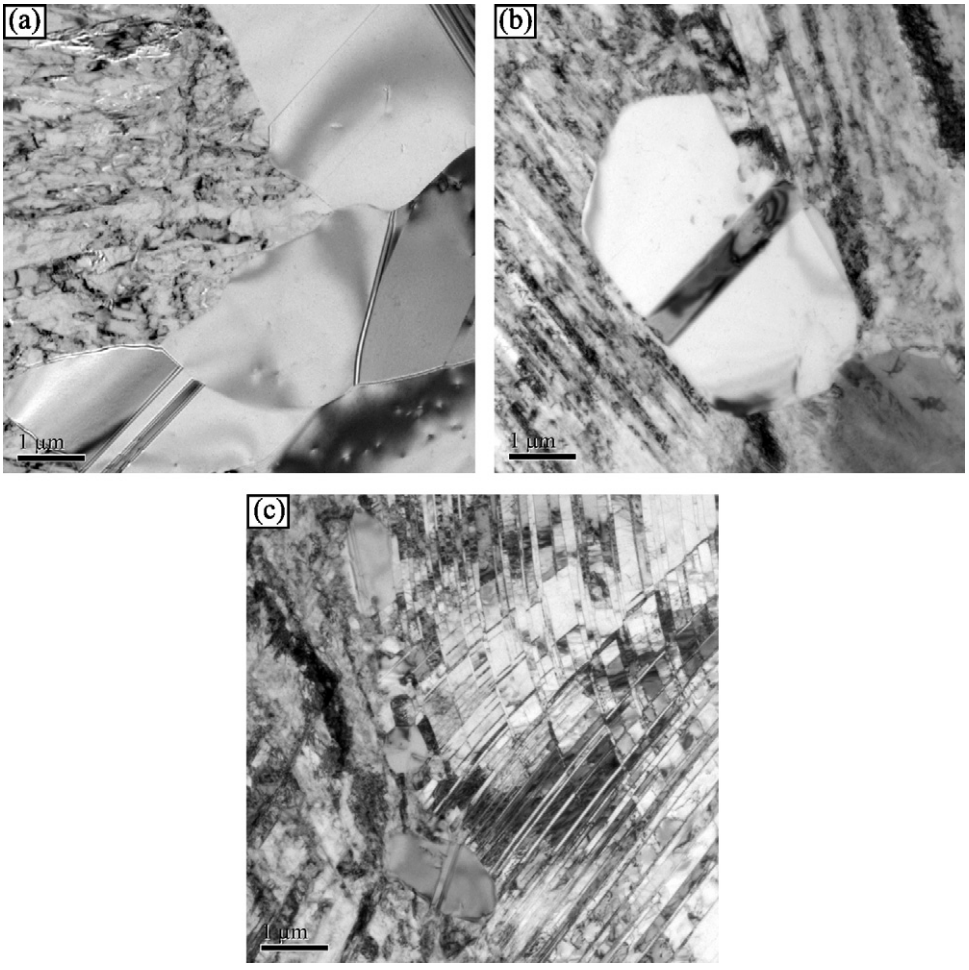

Fig. 5. TEM bright field images of the specimens deformed at 1150 °C and (a) at a strain rate of 2.5 s^{-1} and engineering strain of 45%, (b) at a strain rate of 5 s^{-1} and engineering strain of 35%, (c) at a strain rate of 7.5 s^{-1} and engineering strain of 30%.

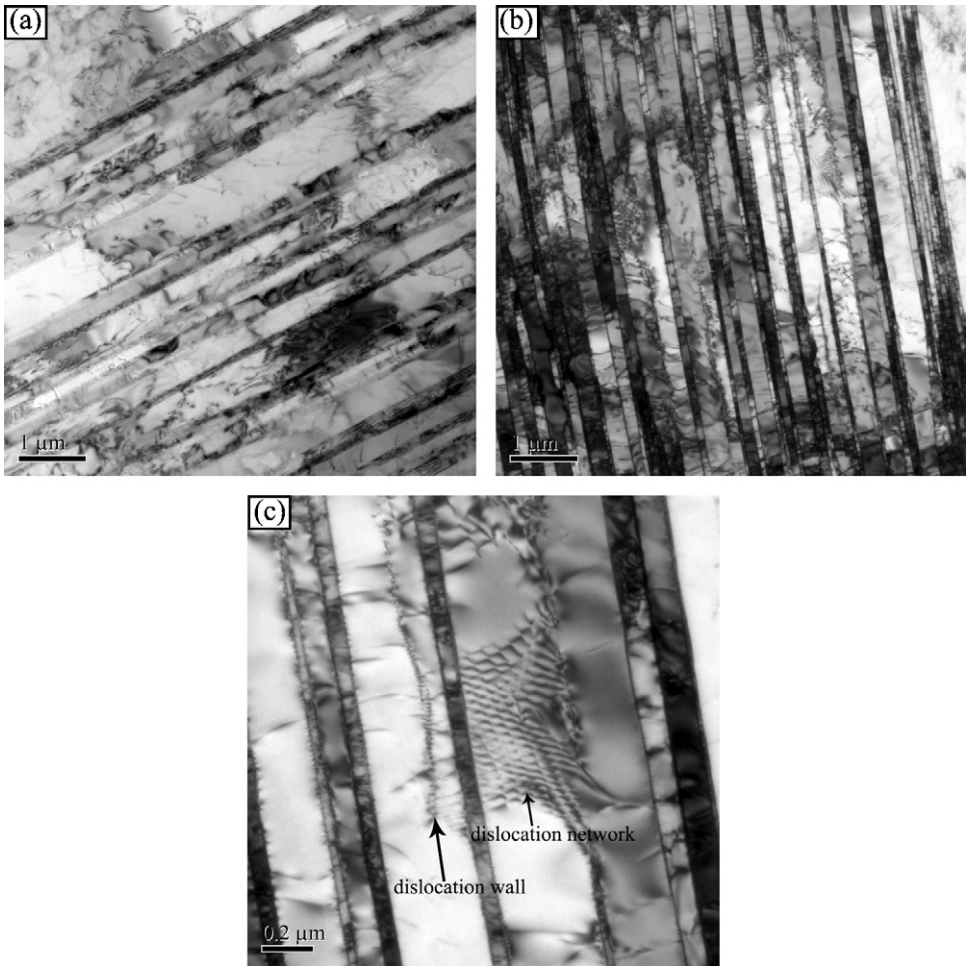

Fig. 6. TEM bright field images of lamellar colonies deformed at 1150 °C and (a) at a strain rate of 2.5 s^{-1} and engineering strain of 45%, (b) at a strain rate of 7.5 s^{-1} and engineering strain of 30%, (c) a magnified view showing lamellar colonies at a strain rate of 7.5 s^{-1} and engineering strain of 30%.

A peak flow stress exists in each curve, which suggests that DRX occurred during the hot deformation and the work softening is mainly caused by DRX. Furthermore, the flow stresses increase with increasing strain rate and decreasing deformation temperature. It is because plastic deformation cannot fully complete in some regions in the shortening of required time of unit strain during deformation and the flow stresses ascending. And higher temperature brings about enhancement of thermal activation, decrease of atomic critical shear stress and increase of softening degree of the alloys.

3.3. Microstructural evolution

Fig. 3 presents the EBSD orientation maps of the samples deformed under different deformation conditions. The color codes in the EBSD maps indicate the orientations of the α_2 and γ grains at different crystallographic directions, respectively. It can be clearly seen that the grain size decreases with increasing strain rate. Fine recrystallized grains are developed along the initial grain boundaries at both of the deformation conditions (Fig. 3a and b). In Ti–47Al–2Cr–0.2Mo alloy, the deformed microstructure is mainly comprised of bending, fracturing and DRX grains. DRX preferential nucleation occurs at triple junctions. These fine DRX grains can promote boundaries movement and grains rotation during the deformation. As a result, the flow stress decreases and the alloys tend to soften (Fig. 2). Large deformation can be obtained and hot deformability is improved.

In order to investigate the effect of deformation strain rate on the orientations of grains and subgrains, samples deforming under different deformation conditions were analyzed by EBSD. Fig. 4a and b shows the distributions of misorientation angles at different strain rates calculated from EBSD results. It can be seen that the fraction of low angle boundaries (<15°) increases with increasing strain rate, because the low angle boundaries do not have enough time to transit from low angle to high angle boundaries (>15°) at a strain rate of 7.5 s^{-1} and engineering strain of 30%. However, it is obvious that the percentage of high angle boundaries is the function of grain boundaries. The reason is that even the newly formed DRX grains are very small but they have high angle boundaries. Fig. 5a–c shows the TEM bright field images of the specimens deformed with different strain rates at the temperature of 1150 °C. The fine DRX grains distribute at the original grain boundaries, as seen from Fig. 5a–c, and the DRX grain size decreases with increasing strain rate. The condition for the growth of a DRX grain is thought to be dependent on the distribution and density of dislocations. The decrease of the strain rate would lead to a decrease in the critical dislocation density, and then lower the critical strain for the occurrence of DRX. Therefore, at the lower strain rate, the DRX nuclei have enough time to develop, whereas the growth of DRX grains is inhibited at the higher strain rate.

Previous study has demonstrated that the differences in nucleation processes of DRX might be related to deformation temperature and strain rate [11]. In the Ti–47Al–2Cr–0.2Mo alloy DRX preferential nucleation occurs at grain boundaries (Fig. 5c), and dif-

ferent DRX mechanisms have been proposed for TiAl-based alloys. Skrotzki et al. [17] indicated that nucleation and growth took place in highly deformed regions of Ti–47Al–2Mn–2Nb+0.8 vol.% TiB_2 because of the low stacking fault energy. Fukutomi et al. [18] reported that strain-induced grain boundary migration had been assumed for compressed Ti–49Al because of maintenance of the deformation texture and continuous strengthening of the texture. It is suggested that all the mechanisms are the main reasons for DRX of Ti–47Al–2Cr–0.2Mo alloy.

Fig. 6a–c shows the bright field TEM images taken from the lamellar colonies region of Ti–47Al–2Cr–0.2Mo alloys deformed under different deformation conditions. It is evident that the average interlamellar spacing at a strain rate of 7.5 s^{-1} (Fig. 6b) is much finer than that at a strain rate of 2.5 s^{-1} (Fig. 6a) at the temperature of 1150 °C. Oehring et al. [19] found that the deformation properties of TiAl-based alloys were sensitive to microstructures and depend on morphological parameters of lamellar colonies in particular. As shown in Fig. 6 in this study the interlamellar spacing is finer at higher strain rate. It is known that the discontinuous coarsening of the lamellar is mainly controlled by the grain boundary migration. At higher strain rate, the atomic diffusion is suppressed, which leads to a higher driving force of lamellar coarsening. A finer interlamellar spacing is thus obtained. The fine interlamellar spacing is beneficial to mechanical property, but it is not good for high temperature deformability. As seen from Fig. 1, the largest engineering compressive strain decreases from 45% to 25% with increasing strain rate from 2.5 s^{-1} to 7.5 s^{-1}. The main reason is that the fine interlamellar spacing does not provide enough space for dislocations to climb and slide. High densities of dislocations form dislocation walls and networks (Fig. 6c) which are the main reason for baffling deformation, and dislocation tangle may bring external and internal cracks.

4. Conclusions

In this paper, high temperature deformability and microstructural evolution of Ti–47Al–2Cr–0.2Mo alloy were studied. It has been shown that the largest engineering compressive strain of the alloy increases with decreasing strain rate and increasing deformation temperature. The flow stresses increase with increasing strain rate and decreasing deformation temperature. High temperature deformation mechanism of Ti–47Al–2Cr–0.2Mo alloy mainly refers to the bending, fracturing and DRX, and DRX preferential nucleation occurs at triple junctions. It is also evident that the average interlamellar spacing at a strain rate of 7.5 s^{-1} is much finer than that of at a strain rate of 2.5 s^{-1} at a temperature of 1150 °C.

Acknowledgment

This work is supported by Hi-Tech Research and Development Program of China (2008AA03A233).

References

[1] X. Lu, X.B. He, B. Zhang, X.H. Qu, L. Zhang, Z.X. Guo, J.J. Tian, J. Alloys Compd. 478 (2009) 220–225.
[2] W.F. Cui, C.M. Liu, J. Alloys Compd. 477 (2009) 596–601.
[3] Z.W. Huang, Scripta Mater. 52 (2005) 1021–1025.
[4] Y.H. Wang, J.P. Lin, X.J. Xu, Y.H. He, Y.L. Wang, G.L. Chen, J. Alloys Compd. 458 (2008) 313–317.
[5] D. Hu, X. Wu, M.H. Loretto, Intermetallics 13 (2005) 914–919.
[6] Y.Y. Chen, F. Yang, F.T. Kong, S.L. Xiao, J. Alloys Compd. 498 (2010) 95–101.
[7] A. Couret, G. Molénat, J. Galy, M. Thomas, Intermetallics 16 (2008) 1134–1141.
[8] X.M. He, Z.Q. Yu, G.M. Liu, W.G. Wang, X.M. Lai, Mater. Des. 30 (2009) 166–169.
[9] S.L. Semiatin, V. Seetharaman, I. Weiss, Mater. Sci. Eng. A 243 (1998) 1–24.
[10] S.S. Li, X.K. Su, Y.F. Han, X.J. Xu, G.L. Chen, Intermetallics 13 (2005) 323–328.
[11] F.T. Kong, Y.Y. Chen, B.H. Li, Mater. Sci. Eng. A 499 (2009) 53–57.
[12] C.T. Liu, P.J. Maziasz, Intermetallics 6 (1998) 653–661.
[13] G. Fanta, R. Bohn, M. Dahms, T. Klassen, R. Bormann, Intermetallics 9 (2001) 45–49.
[14] R. Bohn, T. Klassen, R. Bormann, Intermetallics 9 (2001) 559–569.
[15] G.A. Salishchev, R.M. Imayev, O.N. Senkov, V.M. Imayev, N.K. Gabdullin, M.R. Shagiev, A.V. Kuznetsov, F.H. Froes, Mater. Sci. Eng. A 286 (2000) 236–243.
[16] X.J. Xu, J.P. Lin, Y.L. Wang, Z. Lin, G.L. Chen, Mater. Sci. Eng. A 416 (2006) 98–103.
[17] B. Skrotzki, T. Rudolf, A. Dlouhy, G. Eggeler, Scripta Mater. 39 (1998) 1545–1551.
[18] H. Fukutomi, K. Aoki, S. Takagi, M. Nobuki, H. Mecking, Taichi Kamijo, Intermetallics 2 (1994) 37–42.
[19] M. Oehring, F. Appel, P.J. Ennis, R. Wagner, Intermetallics 7 (1999) 335–345.